Batteries & Supercaps

Research Article
doi.org/10.1002/batt.202300213

Chemistry Europe
European Chemical Societies Publishing

www.batteries-supercaps.org

VIP *Very Important Paper*

Photo-generated Charge Trapping in Phase Segregated Halide Perovskites – A Comprehensive Approach towards Efficient Photo-Rechargeable Ion Capacitors

Tanuj Kumar[+],[a] Ankush Kumar[+],[a, b] Shivang Beniwal,[a] Ramesh Kumar,*[a, c] and Monojit Bag*[a, d]

The right balance between photo-absorption and electronic-ionic conductivity is needed for photo-rechargeable bifunctional devices for off-grid energy applications. Recently halide perovskites have been utilized for photo-rechargeable supercapacitors, but the mechanism of photo-capacitance enhancement is not known. Herein, we have fabricated mixed halide perovskites-based photo-rechargeable supercapacitors in two ways and examined the energy harvesting and storage capabilities of these devices. The porous electrode prepared from the mixed halide perovskites ($CH_3NH_3PbBr_2I$) shows photo-capacitance enhancement up to 15 F/g, while the electrode prepared from the blend of $CH_3NH_3PbBr_3$ and $CH_3NH_3PbI_3$ (2:1 by molar ratio) shows the photo-capacitance diminution up to 12 F/g. Despite higher specific capacitance (~38 F/g in dark) in blend perovskites due to increased ion diffusion, the photo-generated charge trapping at nanoscale phase segregation is responsible for the diminution in photo-capacitance of these bifunctional devices, while a uniform mixing of halide ions in mixed halide perovskites nanocrystals leads to increased photo-capacitance.

Introduction

Bifunctional energy harvesting and storage devices are in high demand because of their application in the Internet of Things (IoT), smart cities, intelligent remote sensors, and autonomous integrated devices.[1–3] In this direction, a lot of research has been done on the external integration of solar cells with energy storage devices.[4–9] For example, researchers reported the integration of traditional silicon-based- and perovskite-based solar cells (PSC) with a solid-state lithium-ion battery (LIB), a flexible solid-state graphene-based supercapacitor, or a lithium-ion capacitor.[5,7,8] However, this external integration introducing energy losses, poor reproducibility, and reliability as it requires additional electronics to match the output voltage with the energy storage system. Therefore, single smart bifunctional device designs can be realized by fabricating a photo-electrode that can simultaneously harvest and store the energy in a single material. Some recent works have been towards graphitic carbon nitride, vanadium pentoxide/dioxide, and molybdenum disulphide–zinc oxide-based photo-electrodes for photo-rechargeable batteries and ion-capacitors that can directly harvest and store energy without the need for additional photovoltaic devices.[10] Therefore, these devices are the best alternative for self-charging or continuous power supply devices. However, these materials have poor cyclic stabilities, low energy storage capacities, and very low photo-charging conversion efficiency. In addition, the photogenerated charge carriers cannot efficiently transport from photovoltaic materials to energy storage materials due to an energy level mismatch at the materials interface.[11–13] Also, the energy storage material blocks the incident light making the photoactive material less effective for the absorption of photons.[12–14] Therefore, it is necessary to investigate novel advanced materials that concurrently combine photovoltaic and energy storage properties.

In last decades organic-inorganic hybrid halide perovskite materials have been utilized for photovoltaics[15–17] and other optoelectronic applications[18–20] due to extraordinary properties. These materials have shown great promise for the fabrication of efficient energy storage devices for smart applications.[21–26] In this direction, we reported hybrid halide perovskite-based photo-rechargeable supercapacitors that can simultaneously harvest and store energy in a single device.[23] These perovskites are especially well-suited materials for the fabrication of bifunctional photo-electrodes due to their superior optoelectronic properties and tunable electronic-ionic conductivity.[27,28] However, the mechanism of photo-capacitance enhancement in

[a] *T. Kumar,[+] A. Kumar,[+] S. Beniwal, Dr. R. Kumar, Prof. Dr. M. Bag*
Advanced Research in Electrochemical Impedance Spectroscopy Laboratory
Indian Institute of Technology Roorkee
Roorkee 247667 (India)
E-mail: rkumar1@ph.iitr.ac.in
monojit.bag@ph.iitr.ac.in

[b] *A. Kumar[+]*
School of Physics and Mathematical Sciences
Nanyang Technological University Singapore
21 Nanyang link, Singapore 637371 (Singapore)

[c] *Dr. R. Kumar*
Department of Chemistry
Ångström Laboratory
Uppsala University
Box 523, SE, 75120 Uppsala (Sweden)

[d] *Prof. Dr. M. Bag*
Centre for Nanotechnology
Indian Institute of Technology Roorkee
Roorkee 247667 (India)

[+] *These authors contributed equally to this work.*

Supporting information for this article is available on the WWW under https://doi.org/10.1002/batt.202300213

these devices is still not known. The role of halide ions on the charge transport properties needs to be well understood for further optimization to improve the overall efficiency of the device for commercial application.

In this work, we have fabricated mixed halide perovskite photo-electrodes by two different methods which have the potential to integrate photovoltaic and supercapacitor functionalities simultaneously. In the first approach, single crystal of bromide- and iodide-based perovskites ($CH_3NH_3PbBr_2I$) are synthesized before grinding to make perovskite powder. We have referred to these electrodes as mixed-halide perovskite (MHP) electrodes. In the second approach, we have fabricated electrodes using a mechanically synthesize method, in which we have mixed two different halides (Bromide and Iodide) perovskites. Then the appropriate ratio of bromide- and iodide-based perovskite ($2CH_3NH_3PbBr_3 + CH_3NH_3PbI_3$) are mixed to prepare porous electrodes. These perovskite electrodes are referred to as blended perovskite (BP) electrodes. We performed electrochemical measurements in the dark and under illumination conditions to investigate the device performance and the role of different halide phases on the device kinetics. It has been observed that the dark capacitance is significantly higher in the BP photo-electrode than the MHP photo-electrode due to increased ionic conductivity while photo-capacitance decreases upon illumination for the BP photo-electrodes. This might be attributed to the photo-induced phase segregation and charge trapping. On the other hand, the photo-capacitance increases upon illumination for the MHP photo-electrodes. We separated the contributions to the photo-supercapacitor performance made by diffusion-controlled, and capacitive-controlled capacitances using the modified Dunn's Power Law.[29] More interestingly both the electrodes degraded to a similar morphology after 1000 cycles of operation having only photo-capacitance diminution in both the electrodes.

Result and Discussion

Structural characterization

X-ray diffraction (XRD) was performed for the structural analysis of both types of perovskites synthesized powders (BP, MHP).

The XRD patterns of MHP powder display the diffraction peaks at 14.91°, 21.13°, 30.06°, 33.7°, 37.03°, 43.02°, 45.77°, 48.4°, and 53.38° corresponding to reflection planes (100), (110), (111), (200), (210), (211), (220), (300), (310), and (222) of the cubic $CH_3NH_3PbBr_2I$ perovskite. Although $CH_3NH_3PbI_3$ is tetragonal at room temperature, XRD patterns of BP powder display the diffraction peaks at 14.63°, 20.78°, 25.42°, 29.55°, 33.14°, 36.42°, 42.3°, 45.01°, 47.55°, and 52.51° corresponding to reflection planes (100), (110), (111), (200), (210), (211), (220), (300), (310), and (222) similar to the cubic phase of $CH_3NH_3PbBr_2I$ (MHP) perovskite (Figure 1a). To study the detailed structures of both samples, we have analysed the powder XRD peaks of the BP ($MAPbBr_3$ + $MAPbI_3$, 2:1) as well as synthesized single crystals of mixed halide (MHP) samples. BP powder XRD peaks were shifted towards the lower XRD angles. The reflection plane (100) shifted from 14.91° to 14.63°, due to which corresponding lattice constant and pseudo-cubic unit cell volume are increased from 5.93 Å to 6.065 Å and 208.5 $Å^3$ to 223.1 $Å^3$ respectively. This increase in the unit cell will facilitate the ionic movement[30] in the perovskite active layer leading to a higher energy density through charge storage.[31] The average crystallite sizes in both samples are calculated resolving all intense peaks with the use of Scherrer's formula,[25]

$$D = \frac{K\,\lambda}{\beta\,\cos(\theta)} \quad (1)$$

where K is Scherrer's constant = 0.9, λ = 0.15406 nm wavelength of X-ray (Cu_α), β is the FWHM and D gives the average grain size. The XRD peaks of MHP powder are more intense than that of BP powder. The more intense the XRD peaks larger the average crystal size attributed to the homogeneity and fewer defects in crystallinity. The average grain size for MHP powder is 50.05 nm which is reduced to 19.96 nm for BP powder. After depositing the samples on the graphite sheet, the electrode was heated for two hours at 90^0 C, which increased the potential of phase segregation caused by ion migration. It is evident from the XRD curves of the BP electrode and MHP electrode that the BP electrode has two peaks, which clearly demonstrate the phase segregation in the BP electrode, but the MHP electrode has only one peak, which clearly indicates no phase segregation as shown in Figure 1(b). This is because of the nanoscale phase segregation of bromide and iodide ions in the BP-sample, while MHP-sample is more isotropic as shown schematically in Figure 1(c and d) respectively. Energy Dispersive X-Ray Analysis (EDX) of BP sample also shows the Br-rich and I-rich region as shown in Figure 1(e). However, both iodine and bromine are present in most of the regions indicating efficient diffusion of halide ions in BP electrode. EDX mapping of fresh MHP sample does not show any phase segregation (see Supporting Information Figure S1).

Photo-electrochemical measurements

We have performed all the electrochemical measurements on a three-electrode system (Auto-lab potentiostat/galvanostat electrochemical analyzer). We have performed the cyclic voltammetry (CV), and galvanostatic charge/discharge (GCD) measurements in both dark and illuminated (white light source, 20000 LUX) conditions and investigated the electrochemical performance for both electrodes. These electrochemical measurements were performed in a typical close beaker cell consisting of the three electrodes (Platinum (Pt), Ag/AgCl, working electrode) in (0.1 M) tetrabutylammonium tetrafluoroborate electrolyte in dichloromethane (DCM) solvent as shown in Supporting Information Figure S2. The cyclic-voltammetry (CV) measurement for both electrodes is carried out in dark and illuminated conditions at different scan rates varying from 5 $mV\,s^{-1}$ to 160 $mV\,s^{-1}$ (see Supporting Information Figure S3). Figure 2(a and b) displays the CV plots for both the electrodes, i.e., MHP and BP at a scan rate of 5 $mV\,s^{-1}$. We observed a significant

Research Article
doi.org/10.1002/batt.202300213
Chemistry Europe
European Chemical Societies Publishing

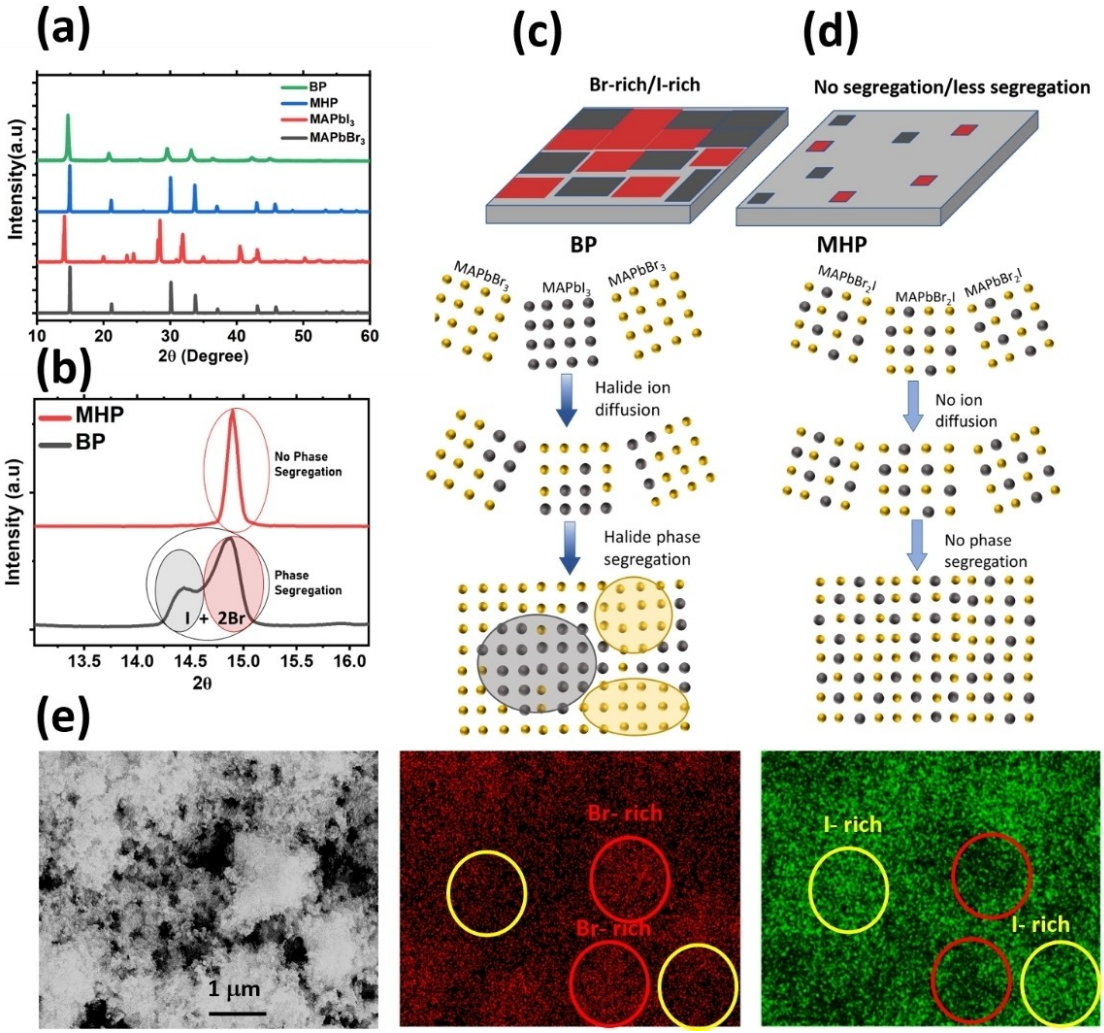

Figure 1. a) XRD patterns for the powder of the Blended perovskite (BP), Mixed-halide perovskite (MHP), $CH_3NH_3PbBr_3$, and $CH_3NH_3PbI_3$. b) Comparison of the most intense XRD peak of MHP-electrode and BP-electrode. Schematic illustration of halide phase segregation of c) BP and d) MHP, and e) energy dispersive X-ray analysis (EDX) mapping of BP sample shows the Br-rich and I-rich region.

change in capacitance under light for both electrodes. The capacitance for the MHP photo-electrode is increased from 26.85 F g^{-1} to 30.41 F g^{-1}, while, for the BP photo-electrode the capacitance is decreased from 38.7 F g^{-1} to 33.1 F g^{-1} when white light is illuminated using three-electrode system. However, for practical application the measurement should be carried out in two-electrode systems. The measurement is carried out by shorting reference and counter electrode to Pt-electrode while perovskite electrode as working electrode. The calculated maximum value of energy density is 0.9 and 0.7 Wh kg^{-1} for BP and MHP electrode respectively at 85 mA g^{-1} current density as shown in Supporting Information Figure S4. From GCD spectra of both electrodes under dark and light conditions, we can see that the porous of MHP shows photo-capacitance enhancement up to 15 F g^{-1}, while the electrode prepared from the blend of $CH_3NH_3PbBr_3$ and $CH_3NH_3PbI_3$ (2 : 1 by molar ratio) shows the photo-capacitance diminution up to 12 F g^{-1} at current density of 0.23 mA g^{-1} (see Figure 2c, d, f). The GCD spectra of both electrodes at different current density are given in the supporting information (see Supporting Information Figure S5). We also observed that photo-capacitance enhancement in MHP electrode decreases with the increasing voltage scan rate as well as photo-capacitance diminution in BP electrodes decreases with the increasing voltage scan rate (Figure 2e, f). Hence it can be concluded that the photo-capacitance enhancement or diminution is dependent on the electronic-ionic coupling and their kinetics.[32,33] At a slower scan rate the electronic current is strongly coupled with the ionic current of the electrode due to coherent ion migration, while at higher scan rate the ionic current is lagging the electronic current giving rise to inductive effect. The overall capacity of the device decreases with the increasing scan rate. Different synthesis methods play an important role in the photo-capacitance performance of photo-rechargeable supercapacitors due to different morphology of the photo-electrodes. For the BP photo-electrodes, $CH_3NH_3PbBr_3$ and $CH_3NH_3PbI_3$ perovskite powders are mixed in a molar ratio of 2 : 1. Therefore, the inter-diffusion of bromide and iodide ions when individual

Research Article
doi.org/10.1002/batt.202300213
Chemistry Europe
European Chemical Societies Publishing

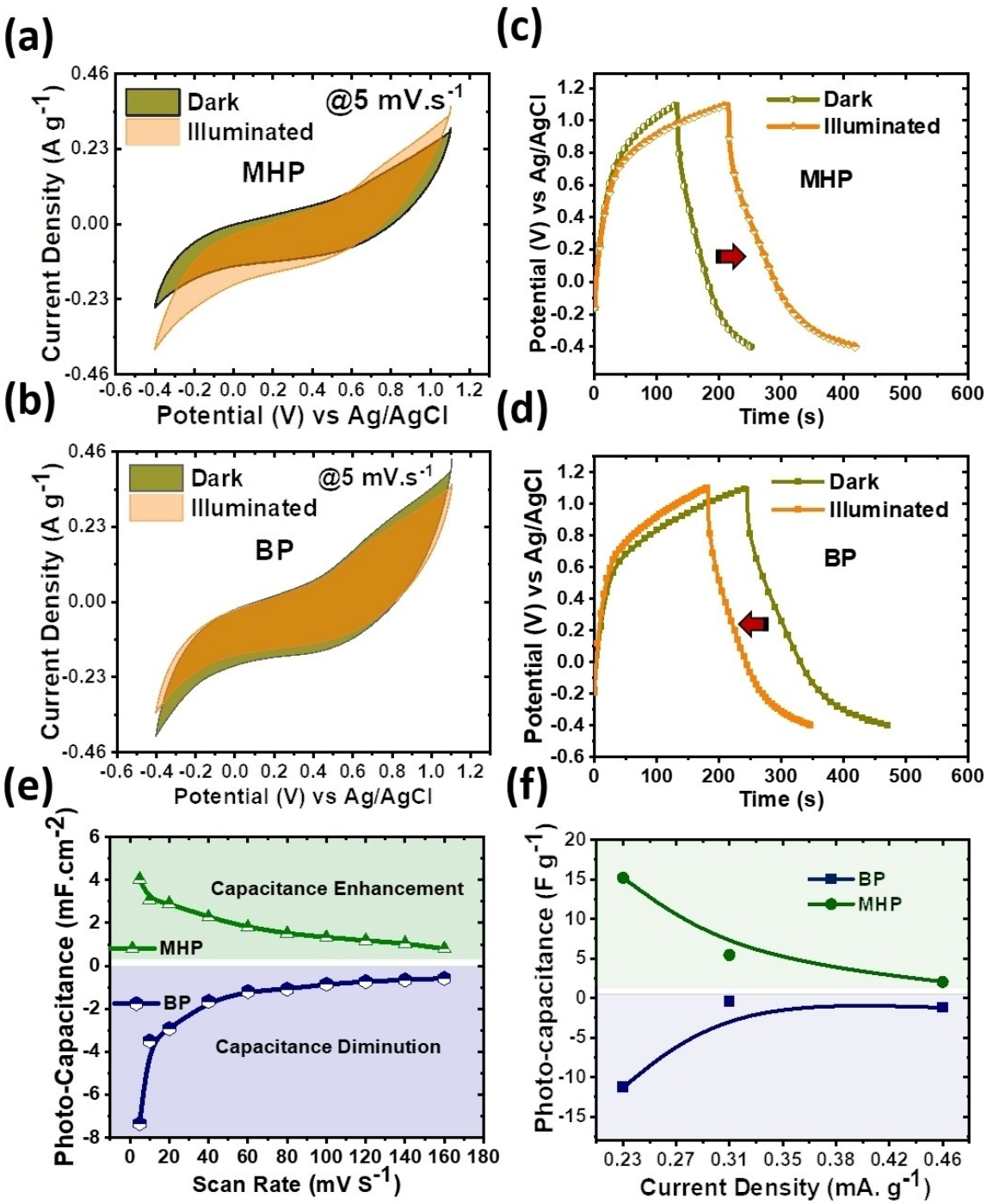

Figure 2. a and b) Cyclic voltammetry curves at 5 mV s^{-1}, and c and d) Galvanostatic charge-discharge curves under dark (green) and illuminated (brown) conditions (15 mW cm^{-2}) for a and c) devices MHP, and b and d) BP devices. The curve between the Photo capacitance and e) scan rate for the enhancement and diminution of the capacitance under light for both devices. f) The photo-capacitance of BP electrode and MHP electrode with the increasing voltage scan rate.

nanocrystals are mixed, can result in nanoscale phase segregation of the mixed halide perovskites to form bromide-rich and iodide-rich regions as shown in Figure 1(e).[34] The long diffusion length and life time in perovskites allow photogenerated charge carriers to move in a greater volume fraction inside the bulk of the material before recombining. The I-rich region has a lower band gap compared to Br-rich regions, therefore the electrons are more likely to get trapped in I-rich regions, while holes from the Br-rich region can also move thermally to the I-rich region and get recombined with the electrons.[34,35] Therefore, the presence of mixed phase nanoscale domains form non-aligned energy band levels (conduction band/valance band) that cause the energy bands mismatch, this mismatch of bands leads to poor separation and transportation of photo-

Research Article
doi.org/10.1002/batt.202300213
Chemistry Europe
European Chemical Societies Publishing

generated charge carriers due to trapping that limits the overall photo charge conversion efficiency. The mechanism of photo-generated charge carrier in the MHP electrode- and BP electrode are shown in the schematic in Figure 3(a and b). There is no or less trapping of photo-generated charge carriers in the MHP photo-electrodes due to homogeneous mixing of bromide and iodine perovskites nanocrystals (Figure 3a). However, in the BP electrode devices as shown in Figure 3b, the conduction band of the iodide-rich perovskite phase lying below the conduction band of the bromide-rich phase causes the movement of the photo-generated electrons toward the iodide-rich domains. The electrons generated in both types of phases can be trapped in the conduction band of the I-rich domain surrounded by the Br-rich domain causing diminished capacitance upon illumination.

Additionally, we performed GCD cycle tests under illumination, charging without any external bias at 0 A g^{-1} and discharging at 0.025 A g^{-1} in order to assess the energy harvesting and storage capabilities of photo-electrodes concurrently. For the light sources we have used white light with low intensity 1500 LUX (referred as 1st source) and blue light source of 405 nm at 90 mW cm^{-2} (referred as 2nd source). The carbon black content of the fresh electrode was reduced to 2% in order to calculate photo-capacitance only due to active perovskite electrodes, having mass loading of 2 mg. To prevent carbon from absorbing photons during illumination, the carbon content has been decreased. According to Figure 4, we separated the GCD curves into four separate regions, with regions (I) and (IV) in the 1st source ($<$ 1500 LUX) and regions (II) and (III) in the 2nd source (blue light illumination) for the MHP-electrode. The photovoltage of the MHP photo-electrode is around 491 mV (region-I) and 860 mV (region-II) under the illumination of 1st source and 2nd source respectively, without using any bias, photo-charging is 75% greater under 2nd source illumination in comparison 1st source as shown in Figure 4(a). Due to the electrons and ions' reaction to the high energy photons, which have the ability to affect the energy storage, the potential changes when it is illuminated. The charge storage in perovskite-based energy storage, such as photo-rechargeable supercapacitors, may be aided by the free charge carriers under light. We have shown the regions of the BP-electrodes that was charged and discharged at the same rate as the MHP electrode, regions (I) and (II) under 1st source illumination, (III) and (IV) under 2nd source illumination and in the same optical environment. However, for the BP-electrode the photo-voltage was found to be 464 mV and 404 mV under low light and blue light condition which clearly shows a loss in the photo-voltage reduced by 12.4% in blue illumination. This drop in photo-voltage is clear evidence that the photo charge carrier was trapped in the I-rich area, which causes the capacitance to drop from 20.7 F g^{-1} under low light intensity to 15.42 F g^{-1} (25% less) under blue light illumination as shown in Figure 4(d). To measure the impact of the illumination on the MHP-electrode's active area, we conducted an experiment for the same MHP-electrode after ~2 hr of illumination in which the area of the illumination was varied (50%, 80% and 100% area) while maintaining the same charging and discharging rates. According to Supporting Information Figure S6, higher photo-voltage was seen as the region of illumination was increased. This may be because the photo-charge carrier increased as the illuminated area of the active electrode increased. When the whole electrode was illuminated, the photo-voltage rose from 160 mV (when the illuminated portion of the electrode is 50%) to 649 mV (when the illuminated portion of the electrode is 100%). This little decreased value of photovoltage after two hours of illumination may be the result of degradation of the perovskite based electrode due to continuation illumination time while measurements are being made. So, we can conclude that under continuous blue light illumination for 2hr causes the degradation of the perovskite electrode due to ion migration (see Supporting Information Figure S6). The photo-energy density and power-density of the MHP electrode are ~1.608 Wh kg^{-1} and 10.36 W kg^{-1}, respectively under the illumination of the 1st source and 2nd source (90 mW cm^{-2} with

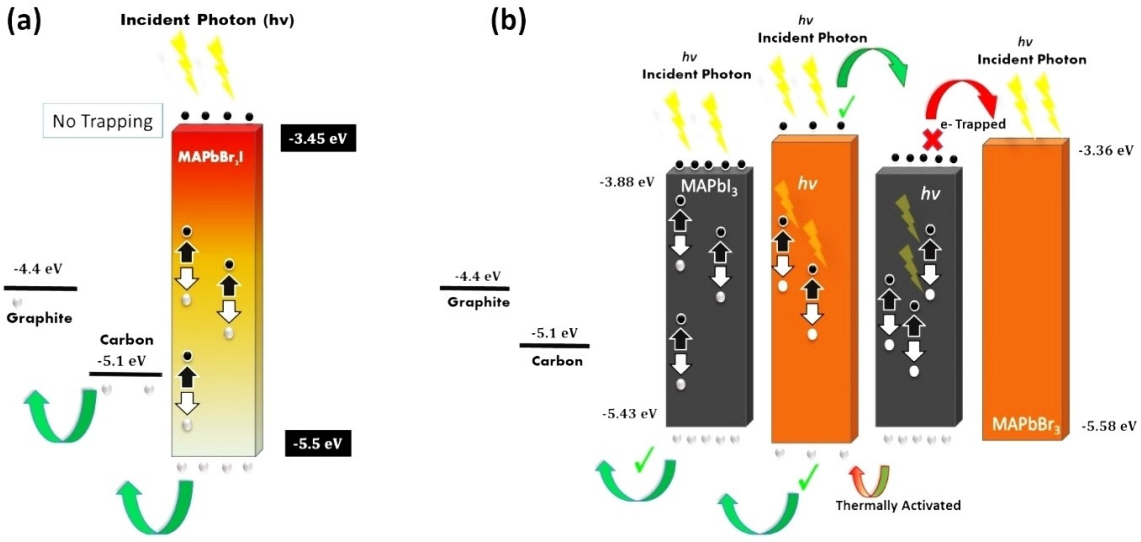

Figure 3. Energy band diagram of a) illuminated mixed halide perovskite (MHP) and b) Phase segregated blended perovskite (BP).

Research Article
doi.org/10.1002/batt.202300213
Chemistry Europe
European Chemical Societies Publishing

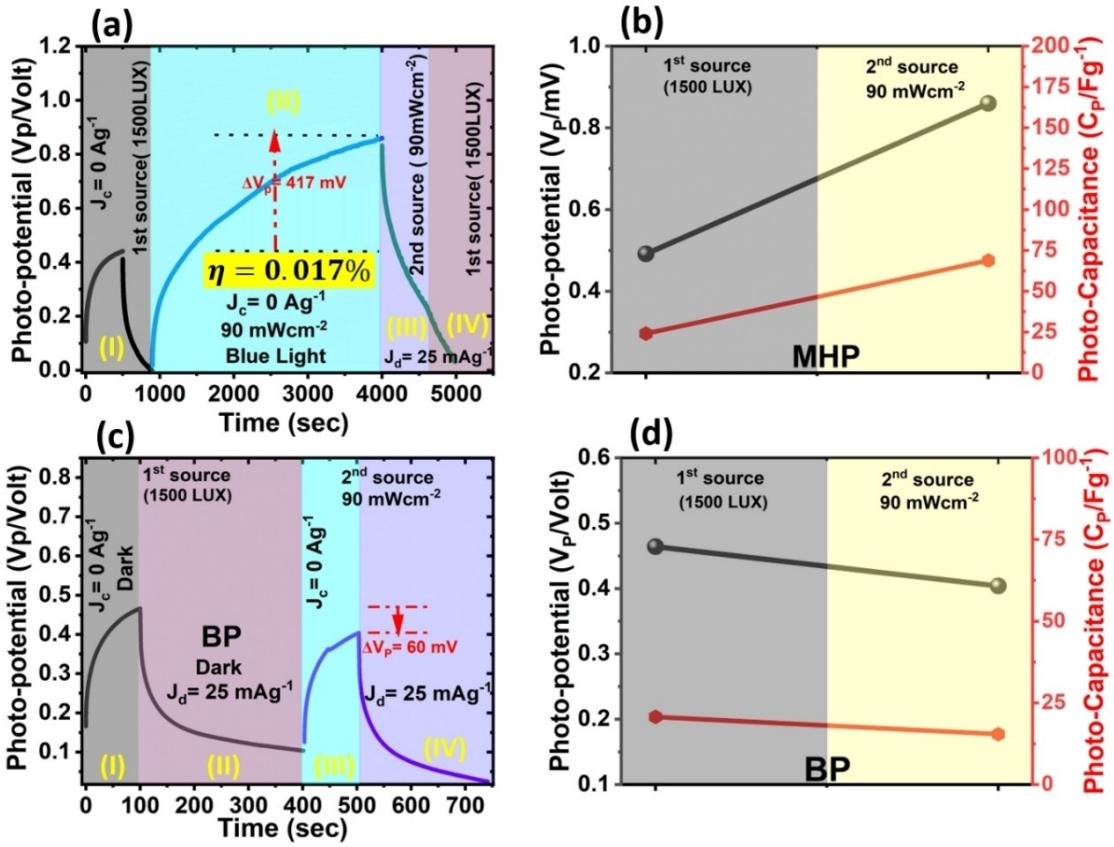

Figure 4. GCD measurements under low light (1500 LUX) and illumination conditions (blue light, 90 mW cm^{-2}) without applied current (J_c = 0 A g^{-1}) and discharging at J_d = 25 mA g^{-1} for a) MHP- electrode and c) BP-electrode. The comparison between the value of the photo-potential and photo-capacitance under 1st source (low light) and 2nd source (90 mW cm^{-2}) illuminated condition for b) MHP-electrode and d) BP- electrode.

405 nm wavelength), when calculated using three-electrode setup. On the other hand, there is no photo-charging response of the BP electrodes as shown in Figure 4(d) and the energy density is decreased from 0.372 Wh kg^{-1} (under 1st source) to 0.315 Wh kg^{-1} (2nd source). The photo-capacitance value is increased from 24.04 F g^{-1} under 1st source to 43.87 F g^{-1} under illumination of the 2nd source for the MHP-electrode. Increasing capacity with the increasing light intensity indicates that the photo-voltage is responsible for the charging of the super-capacitors. Through these measurements, the charge accumulated throughout the light-charging process can be quantified, and the photo-conversion efficiency of the photo-supercapacitors may be determined (for 405 nm blue illumination). The calculated value of the photo-conversion efficiency is 0.017% which is one of the best values found for the supercapacitor based on the perovskite-electrode. However, we believe that this efficiency can be increased by altering the bandgap, absorption, composition of the electrode and by tuning the optical properties of the perovskite material. GCD measurements under low light conditions (1500 LUX) and other wavelengths including green, blue and UV light is shown in Supporting Information Figure S7.

Ensuring long-term stability is a critical aspect that needs to be addressed. Therefore, one thousand cycles of cyclic voltammetry (CV) measurements at a scan rate of 80 mV/s are conducted to assess the cyclic stability of both electrodes in our study. It was observed that MHP electrode exhibited some instability, as it reached its maximum capacity value after approximately 950 cycles (See Supporting Information Figure S8). This observation suggests that the electrode may have undergone an initial activation or conditioning process, which took some time to stabilize and activates the pores. This leads to an increased participation of electrolytic ions in the electrochemical reaction, resulting in enhanced capacitance. On the other hand, the BP electrode demonstrated a peak capacity after around 300 cycles and subsequently showed signs of degradation. This behaviour can be attributed to the absence of a binder in both the electrodes, which is typically used to enhance the mechanical stability of the electrode.

As both the electrodes are found to be unstable after several cycles of operation, iodine expulsion from the electrode leads to mostly Br-rich morphology along with the mixed halide-perovskite phase as shown in Figure 5(a and b). A broad peak appears at 15.46° corresponding to the (100) peak of $CH_3NH_3PbBr_3$ cubic phase (see Supporting Information Figure S9). Br-rich phase is highly disordered and under tensile stress as a skewed broadening is observed towards lower diffraction angle. Relative intensity of (100) peak for $CH_3NH_3PbBr_3$ and $CH_3NH_3PbBr_2I$ in both samples indicates that the iodine repulsion in BP electrode is more as compared to

Research Article
doi.org/10.1002/batt.202300213
Chemistry Europe
European Chemical Societies Publishing

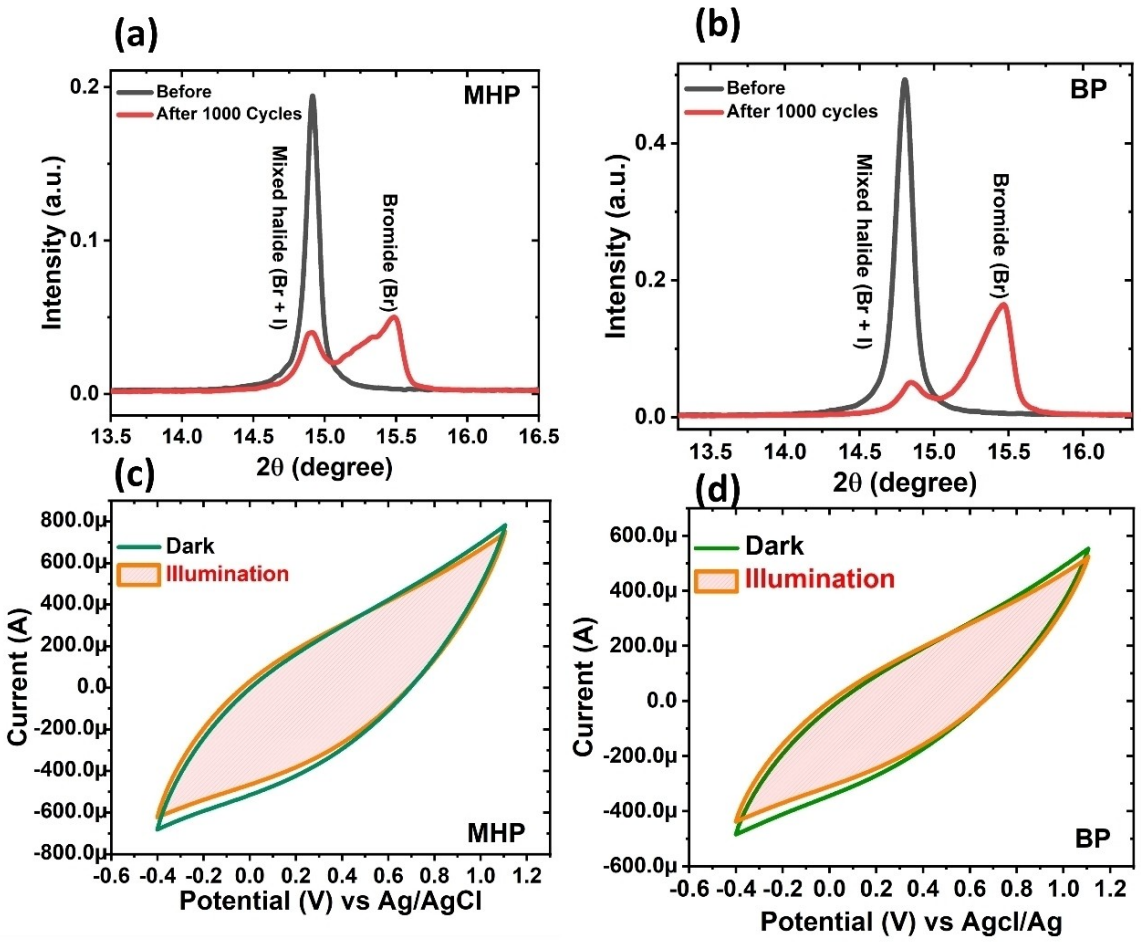

Figure 5. The 100 XRD peak of a) MHP-electrode and b) BP-electrode before and after 1000 cycles in cyclic voltammetry. The CV measurement under dark and illumination after 1000 cycles in cyclic voltammetry for c) MHP-electrode and d) BP-electrode.

MHP electrode. This is also confirmed from the spectro-electrochemistry measurement of the electrolytes (see Supporting Information Figure S10) where a strong absorption peak at around 365 nm corresponding to I_3^- generation is observed.[36] Interestingly both electrodes show photo-capacitance diminution after 1000 cycles of operation as shown in Figure 5(c and d). In the EDX mapping two distinct regions of I-rich and Br-rich domains in the MHP electrode can be seen after cycling. This observation demonstrates the occurrence of phase segregation within the MHP material (see Supporting Information Figure S1). It is to be noted that the photo-charging disappears once there is phase segregation in MHP sample as well. Our results demonstrate how structural transformations during phase segregation have a dramatic effect on the photo-capacitance as a result of charge carrier trapping and de-trapping.

Charge storage mechanism/ Dunn power law

To further analysis of various charge storage mechanisms in both perovskite photo-electrodes, we calculated the b-value from the Dunn power law given below,[29]

$$i = k\nu^b \quad (2)$$

where, i is the current response (A/g), b is the power law parameter, and k is the proportionality constant. Theoretically, $b = 0.5$ is associated with the diffusion-limited charge storage mechanism and $b = 1$ is associated with the electric double-layer capacitance (EDLC) mechanism. In perovskite-based electrochemical cells, the b value exceeds unity ($b > 1$) at the applied field due to ion migration in perovskite that modifies the net potential across the perovskite active layer.[31] In both photo-electrodes, the b values are in the range of $0.25 < b < 0.7$ at higher potentials (> 0.2 V), suggesting the dominating charge storage mechanisms as diffusion-limited due to liquid electrolytic ion intercalation/deintercalation in perovskite photo-electrodes (see Figure 6). At low applied field (< 0.2 V), the b values are in the range of $0.7 < b < 1.0$, indicating a capacitive mechanism due to accumulation of charges at the perovskite-electrolyte interface and pore boundaries. It can be noted that the b value exceeds unity ($b > 1$) at the low-field regime in BP electrodes whereas the b value is within unity ($b < 1$) in MHP electrodes as shown in Figure 6(a and b). Recently, we reported that the b-value is directly related to the ion migration in the perovskite active layer.[31] It can be attributed that the ion

Research Article
doi.org/10.1002/batt.202300213
Chemistry Europe
European Chemical Societies Publishing

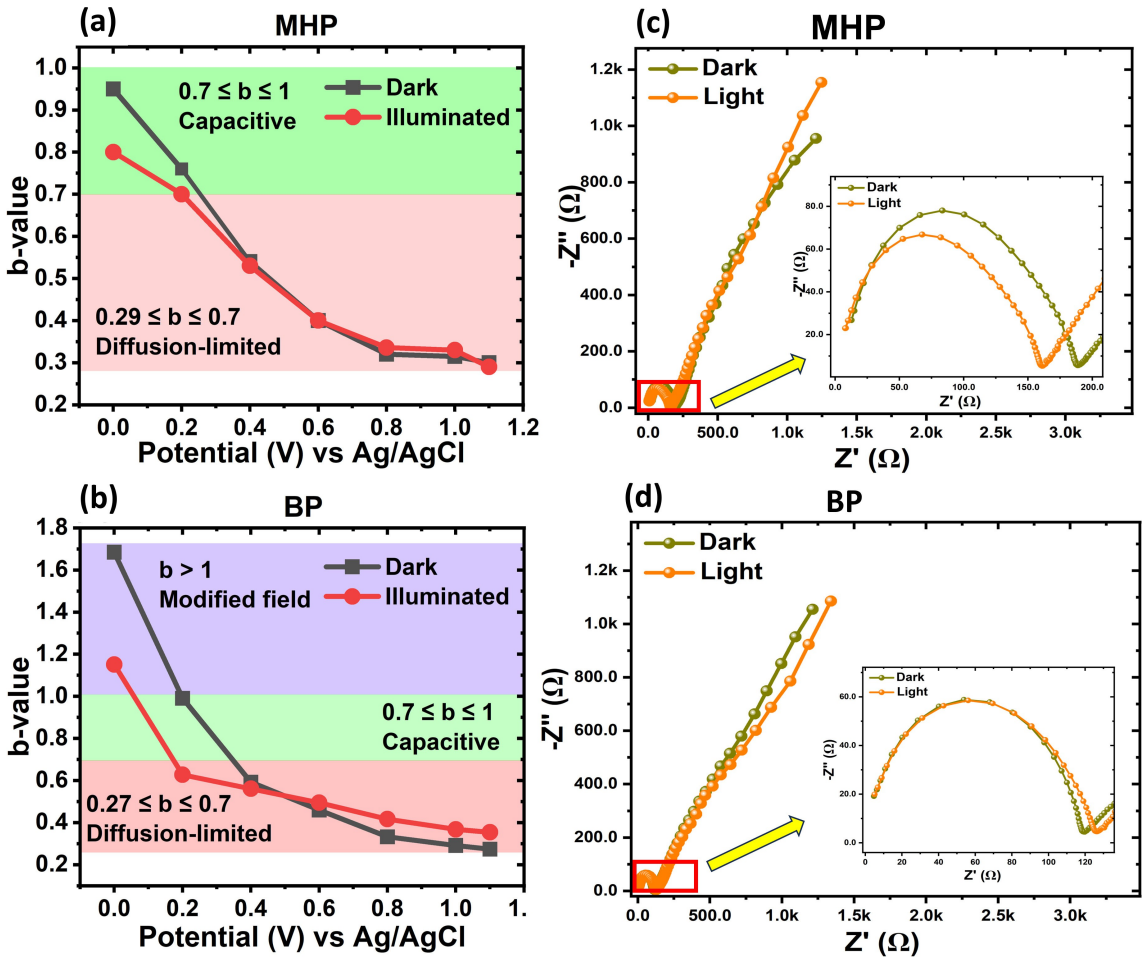

Figure 6. The variation of *b* values with applied potential (versus Ag/AgCl) for A) MHP-electrode and B) BP-electrode. The EIS response measured at 0 V for C) MHP-electrode and D) BP-electrode under dark and illumination.

migration in MHP electrodes is significantly lower than that in BP electrodes mainly due to their uniform mixing of halide ions in perovskite nanocrystals and hence no phase segregation. On the other hand, BP electrode has higher unit cell volume indicating lower activation energy for the ion migration.[18] Furthermore, we have separated out the relative contribution of the diffusion-limited and capacitive (EDLC) processes by deconvolution the voltametric current response (Dunn equation) into two components according to our previous published work. The contribution of different charge storage mechanisms of both electrodes under light and dark conditions are given in the Supporting Information Figure S11. On conducting the Electrochemical Impedance Spectroscopy (EIS) using three electrodes set up, our findings reveal that in the case of the BP electrode, the charge transfer resistance increases upon exposure to light, which aligns with the expected behaviour as shown in Figure 6(c and d). In case of MHP electrode, an opposite trend is observed. The charge transfer resistance decreases up on illumination as expected.

Conclusions

In conclusion, we have demonstrated that the synthesis root of halide perovskites plays a significant role in the photo-capacitance performance of photo-rechargeable supercapacitors. The physical intermixing of different halide perovskites powder leads to nanoscale phase segregation in blend perovskites where bromide-rich and iodide-rich domains are interconnected through the mixed phase. The presence of photo-capacitance diminution in blend perovskite photo-electrodes is due to the charge trapping at the iodide-rich domains leading to poor separation and transmission of photogenerated charge carriers. These electrodes also degrade more due to higher iodine expulsion compared to mixed halide perovskite electrodes. However increased ion migration in blend perovskite electrodes increases the storage capacity under dark condition. Mixed halide perovskite photo-electrodes are more isotropic and stable during photo-charging. We have achieved photo-energy density ~0.655 Wh kg^{-1} and ~1.6 Wh kg^{-1} under 1st source of low light illumination (1500 LUX) and 2nd source blue light illumination (90 mW cm^{-2}, 405 nm) for the MHP-electrode respectively. The photo conversion efficiency is found

to be highest with value 0.017%. However, we have achieved photo-energy density ~0.372 Wh kg^{-1} and ~0.3158 Wh kg^{-1} under low light illumination and blue light illumination of power 90 mW cm^{-2} for the BP-electrode, respectively.

Experimental Section

Chemical used

Methylammonium bromide (CH_3NH_3Br, 99.6%, TCI Chemicals), Methylammonium Iodide (CH_3NH_3I, 99.6% TCI Chemicals), lead bromide (II) ($PbBr_2$, 99.9%, Sigma-Aldrich), lead iodide (II) (PbI_2, 99.9%, Sigma-Aldrich), Gamma-butyrolactone (GBL, Sigma-Aldrich) and dimethylformamide (DMF, anhydrous 99.8%, Sigma-Aldrich) were used as received for the synthesis of different single crystals.

Synthesis of MHPs powder

To synthesis active materials the single crystals of $CH_3NH_3PbBr_3$, $CH_3NH_3PbI_3$ and $MAPbBr_2I$ were synthesis by inverse temperature crystallization technique (ITC) in DMF, GBL and Mixture of DMF and GBL respectively. Single crystals were ground for 30–35 minutes to obtain homogeneous powders.

Material characterization

For the structural analysis, we employed an X-ray diffractometer (XRD D8-Advance) for both synthesized perovskite powder (MHP and BP) with Cu $K_\alpha = 1.54$ Å in the angle range of 5°–65°. EDX mapping of both photoactive electrodes was carried out using a field emission scanning electron microscope (FESEM QUANTA 200 FEG).

Electrode preparation and electrochemical characterization

Photo-electrodes were prepared by the slurry method as we reported in our previous work. In this work, we fabricated the two types of mixed halide perovskite-based photo-electrodes – (1) BP electrode and (2) MHP electrode.

Fabrication of BP electrode: We mixed the synthesized powder from single crystals of methylammonium lead tri-bromide ($CH_3NH_3PbBr_3$) and methylammonium lead tri-iodide ($CH_3NH_3PbI_3$) in 2:1 with activated 15% carbon black in N-methyl-2-pyrrolidone (NMP) solvent and stirrer for 10–12 hours to get smooth and homogeneous slurry. Then, the homogeneous slurry was coated on a graphite sheet (1×1 cm^2) uniformly under ambient conditions. The weight of loaded material on the graphite sheet is ~1.3 mg. Now the electrodes were dried in a vacuum oven at 80 °C overnight.

Fabrication of MHP electrode: For this, single crystals of mixed bromide- and iodide-based perovskites ($CH_3NH_3PbBr_2I$) were synthesized before grinding to make perovskite powder. After that, we mixed the perovskite synthesized powder with 15% carbon black in N-Methyl-2-pyrrolidone (NMP) solvent and stirrer for 10–12 hours to get a smooth and homogeneous slurry. Then, the homogeneous slurry was coated on a graphite sheet (1×1 cm^2) uniformly under ambient conditions.

All the electrochemical measurements were performed on a three-electrode system (Auto-lab potentiostat/galvanostat electrochemical analyzer). We used platinum (Pt) as a counter electrode, Ag/AgCl as a reference electrode, and perovskite-based electrodes as a working bifunctional electrode in the electrolyte solution (0.1 M tetrabutylammonium tetrafluoroborate in DCM solvent).

Supporting Information

Supporting Information is included. A PDF file contains EDX mapping of MHP, three electrode photo-electrochemical system, CV measurements at different scan rate, GCD measurements at different current density, Spectro-electrochemistry measurements, and contribution of diffusion limited and EDLC processes.

Acknowledgements

M.B. acknowledges Science and Engineering Research Board (SERB), INDIA under award no. CRG/2021/001744 dated 07/03/2022 for partial support to carry out this research work. T.K., A.K, and R.K. acknowledges Ministry of Education, Government of India for PhD fellowship.

Conflict of Interests

The authors declare no competing financial interests.

Data Availability Statement

The data that support the findings of this study are available from the corresponding author upon reasonable request.

Keywords: inter-diffusion of ions · phase segregation · photo-rechargeable · trapping/de-trapping

[1] B. D. Boruah, B. Wen, M. De Volder, *ACS Nano* **2021**, *15*, 16616–16624.
[2] B. Deka Boruah, A. Mathieson, S. K. Park, X. Zhang, B. Wen, L. Tan, A. Boies, M. De Volder, *Adv. Energy Mater.* **2021**, *11*, 2100115.
[3] B. D. Boruah, B. Wen, M. De Volder, *Nano Lett.* **2021**, *21*, 3527–3532.
[4] T. Berestok, C. Diestel, N. Ortlieb, J. Buettner, J. Matthews, P. S. C. Schulze, J. C. Goldschmidt, S. W. Glunz, A. Fischer, *Solar RRL* **2021**, *5*, 2100662.
[5] X. Zhang, W. L. Song, J. Tu, J. Wang, M. Wang, S. Jiao, *Adv. Sci.* **2021**, *8*, 2100552.
[6] M. Acik, S. B. Darling, *J. Mater. Chem. A* **2016**, *4*, 6185–6235.
[7] Z. Liu, Y. Zhong, B. Sun, X. Liu, J. Han, T. Shi, Z. Tang, G. Liao, *ACS Appl. Mater. Interfaces* **2017**, *9*, 22361–22368.
[8] F. Zhou, Z. Ren, Y. Zhao, X. Shen, A. Wang, Y. Y. Li, C. Surya, Y. Chai, *ACS Nano* **2016**, *10*, 5900–5908.
[9] R. Liu, J. Wang, T. Sun, M. Wang, C. Wu, H. Zou, T. Song, X. Zhang, S. T. Lee, Z. L. Wang, B. Sun, *Nano Lett.* **2017**, *17*, 4240–4247.
[10] B. D. Boruah, A. Mathieson, B. Wen, C. Jo, F. Deschler, M. De Volder, *Nano Lett.* **2020**, *20*, 5967–5974.
[11] S. Ahmad, C. George, D. J. Beesley, J. J. Baumberg, M. De Volder, *Nano Lett.* **2018**, *18*, 1856–1862.
[12] B. D. Boruah, A. Misra, *ACS Appl. Energ. Mater.* **2019**, *2*, 278–286.
[13] O. Nguyen, E. Courtin, F. Sauvage, N. Krins, C. Sanchez, C. Laberty-Robert, *J. Mater. Chem. A* **2017**, *5*, 5927–5933.
[14] B. D. Boruah, B. Wen, S. Nagane, X. Zhang, S. D. Stranks, A. Boies, M. De Volder, *ACS Energy Lett.* **2020**, *5*, 3132–3139.
[15] H. J. Snaith, *J. Phys. Chem. Lett.* **2013**, *4*, 3623–3630.

[16] W. Nie, H. Tsai, R. Asadpour, J.-C. Blancon, A. J. Neukirch, G. Gupta, J. J. Crochet, M. Chhowalla, S. Tretiak, M. A. Alam, H.-L. Wang, A. D. Mohite, *Science* **2015**, *347*, 522–525.
[17] W. Zhang, G. E. Eperon, H. J. Snaith, *Nat. Energy* **2016**, *1*, 1–8.
[18] T. Chiba, S. Ishikawa, J. Sato, Y. Takahashi, H. Ebe, S. Ohisa, J. Kido, *Adv. Opt. Mater.* **2020**, *8*, 2000289.
[19] R. Kumar, P. Srivastava, T. Kumar, M. Bag, *J. Phys. Chem. C* **2022**, *126*, 14305–14311.
[20] L. Zhang, X. Yang, Q. Jiang, P. Wang, Z. Yin, X. Zhang, H. Tan, Y. Michael Yang, M. Wei, B. R. Sutherland, E. H. Sargent, J. You, *Nat. Commun.* **2017**, *8*, 15640.
[21] P. Srivastava, R. Kumar, M. Bag, *Phys. Chem. Chem. Phys.* **2021**, *23*, 10936–10945.
[22] A. Yadav, P. S. Shukla, J. Kumar, G. Das Varma, M. Bag, *Energy Technol.* **2022**, *10*, 2200778.
[23] R. Kumar, A. Kumar, P. S. Shukla, G. Das Varma, D. Venkataraman, M. Bag, *ACS Appl. Mater. Interfaces* **2022**, *14*, 35592–35599.
[24] L. Zhang, J. Miao, J. Li, Q. Li, *Adv. Funct. Mater.* **2020**, *30*, 2003653.
[25] R. Kumar, P. S. Shukla, G. D. Varma, M. Bag, *Electrochim. Acta* **2021**, *398*, 139344.
[26] R. Kumar, M. Bag, *Energy Technol.* **2022**, *10*, 2100889.
[27] E. Shi, B. Yuan, S. B. Shiring, Y. Gao, Akriti, Y. Guo, C. Su, M. Lai, P. Yang, J. Kong, B. M. Savoie, Y. Yu, L. Dou, *Nature* **2020**, *580*, 614–620.
[28] R. Kumar, P. Srivastava, M. Bag, *ACS Appl. Electron. Mater.* **2020**, *2*, 4087–4098.
[29] J. Wang, J. Polleux, J. Lim, B. Dunn, *J. Phys. Chem. C* **2007**, *111*, 14925–14931.
[30] M. Bag, L. A. Renna, R. Y. Adhikari, S. Karak, F. Liu, P. M. Lahti, T. P. Russell, M. T. Tuominen, D. Venkataraman, *J. Am. Chem. Soc.* **2015**, *137*, 13130–13137.
[31] R. Kumar, M. Bag, *J. Phys. Chem. C* **2021**, *125*, 16946–16954.
[32] E. C. Smith, C. L. C. Ellis, H. Javaid, L. A. Renna, Y. Liu, T. P. Russell, M. Bag, D. Venkataraman, *J. Phys. Chem. C* **2018**, *122*, 13986–13994.
[33] P. Srivastava, M. Bag, *Phys. Chem. Chem. Phys.* **2020**, *22*, 11062–11074.
[34] S. G. Motti, J. B. Patel, R. D. J. Oliver, H. J. Snaith, M. B. Johnston, L. M. Herz, *Nat. Commun.* **2021**, *12*, 6955.
[35] J. T. Dubose, P. V. Kamat, *Accounts Mater. Res.* **2022**, *3*, 761–771.
[36] P. S. Mathew, P. S. Mathew, G. F. Samu, G. F. Samu, C. Janáky, P. V. Kamat, P. V. Kamat, P. V. Kamat, *ACS Energy Lett.* **2020**, *5*, 1872–1880.

Manuscript received: May 18, 2023
Revised manuscript received: July 6, 2023
Accepted manuscript online: July 9, 2023
Version of record online: July 26, 2023